

Optical properties of defects in solids via quantum embedding with good active space orbitals

Bryan T. G. Lau,^{1,2} Brian Busemeyer,² and Timothy C. Berkelbach^{1,2, a)}

¹⁾*Department of Chemistry, Columbia University, New York, New York 10027 USA*

²⁾*Center for Computational Quantum Physics, Flatiron Institute, New York, New York 10010 USA*

The study of isolated defects in solids is a natural target for classical or quantum embedding methods that treat the defect at a high level of theory and the rest of the solid at a lower level of theory. Here, in the context of active-space-based quantum embeddings, we study the performance of three active-space orbital selection schemes based on canonical (energy-ordered) orbitals, local orbitals defined in the spirit of density matrix embedding theory, and approximate natural transition orbitals. Using equation-of-motion coupled-cluster theory with single and double excitations (CCSD), we apply these active space selection schemes to the calculation of the vertical singlet excitation energy of a substitutional carbon dimer defect in hexagonal boron nitride, an oxygen vacancy in magnesium oxide, and a carbon vacancy in diamond. Especially when used in combination with a simple composite correction, we find that the best performing schemes can predict the excitation energy to about 0.1–0.2 eV of its converged value using only a few hundred orbitals, even when the full supercell has thousands of orbitals, which amounts to many-orders-of-magnitude computational savings when using correlated electronic structure theories. When compared to assigned experimental spectra and accounting for vibrational corrections, we find that CCSD predicts excitation energies that are accurate to about 0.1–0.3 eV, which is comparable to its performance in molecules and bulk solids.

I. INTRODUCTION

Point defects in solids are a promising platform for single photon emission and quantum information due to their unique electronic structure and associated optical properties.^{1–3} The computational study of the electronic structure of defects in solids requires the use of large clusters to eliminate boundary effects or large supercells to eliminate spurious periodic interactions.^{4–7} These finite clusters or periodic supercells, which may contain hundreds of atoms and thousands of electrons, can be readily studied with density functional theory (DFT) but are much more difficult to study via correlated methods, many of which have computational costs that scale as a high power or exponentially with the number of electrons and basis functions. The high computational cost and local character of point defects motivate the development of various classical or quantum embedding methods,^{8–17} which seek to approximate the result of the full supercell without an explicit calculation at the high level of theory. Analogous observations on large molecules have motivated similar embedding strategies.^{18–23}

The use of an active space is one of the simplest types of quantum embedding, where a mean-field calculation (Hartree-Fock or DFT) on the full system is followed by a correlated calculation with a truncated number of electrons and orbitals. Active-space-based quantum embedding methods are differentiated by the choice of active space orbitals, the enforcement of self-consistency between high-level and low-level calculations, and the method by which electrons and orbitals outside of the active space are accounted for (if at all). For example, one popular approach to the latter uses the constrained random-phase approximation (cRPA)^{15,17,24} to generate screened Coulomb interactions that are used in the high-level active space calculation.

The present work is concerned with the optimal choice of active space orbitals for neutral excited-state calculations, although much of our discussion applies to the general electronic structure of defects in solids. An obvious route to systematic improvement in quantum embeddings is to grow the size of the active space. A “good” method to choose active space orbitals is one whose results converge quickly with increasing active space size. However, the cost of common high-level solvers, such as full configuration interaction (also known as exact diagonalization) precludes a systematic study of this convergence behavior and, therefore, obscures the optimal choice of active space orbitals.

Here, we calculate defect excitation energies using periodic equation-of-motion coupled-cluster theory with single and double excitations (CCSD)^{25,26} as the high-level active space method. Despite storage and compute costs that scale as N^4 and N^6 , respectively—precluding direct application to large supercells in quality basis sets—CCSD calculations can be routinely performed with about 1000 orbitals, allowing us to go systematically beyond minimal active spaces, explore the rate of convergence towards full supercell results, and thereby compare the quality of different methods for choosing active space orbitals. Recent work from our group has found that CCSD yields neutral excitation energies of bulk semiconductors and insulators that are accurate to about 0.3 eV,^{27,28} motivating the present study of defect excitation energies.

II. METHODS

All of our calculations are performed with a single periodic Hartree-Fock (HF) reference determinant. The active space problem is defined using the true Hamiltonian without any effective one- or two-body operators (aside from the usual frozen-core potential), i.e., we require no double-counting corrections and we do not perform any downfolding of transitions outside the active space as done in other frame-

^{a)}Electronic mail: t.berkelbach@columbia.edu

works,^{15,17,29,30} in the context of embedding, this choice mirrors the philosophy of so-called “full cell” dynamical mean-field theory.³¹ The occupied and unoccupied orbital active spaces are defined separately so as not to alter the HF reference. Specifically, we test the use of three active space schemes based on canonical orbitals, localized orbitals, and approximate natural transition orbitals, which are each described next.

A. Canonical orbitals

The simple first choice for an active space is a subset of canonical HF orbitals, i.e., those that diagonalize the Fock matrix. The most important orbitals are assumed to be those with energies closest to the band gap. In this work, the canonical active space is defined by the number of occupied orbitals (equivalently, the number of electrons being correlated) and the number of unoccupied orbitals, and convergence is achieved by taking the limit where both approach the full system size. Here, for ease of comparison, we use the same number of occupied and unoccupied orbitals as selected by the local orbital scheme, described next. Through testing, we found that this manner of addition is relatively good, although alternatives can easily be imagined. For example, information could be incorporated about the character of the canonical orbitals, prioritizing those with high weight on atoms of interest or with the necessary symmetry for a given transition.

B. Localized orbitals

Our second active space choice is motivated by the assumption that defect physics is local in space. Although our choice to preserve the HF reference precludes the use of a popular quantum embedding localizations that mix occupied and unoccupied orbitals, e.g., with maximally localized Wannier functions,^{15,17,32} here we test a method that is qualitatively similar. Specifically, we follow the active space perspective of density matrix embedding theory^{33,34} in its regional embedding formulation, recently introduced by two of us.¹⁴ Regional embedding follows the atomic valence active space approach,³⁵ but targets a larger space of unoccupied orbitals, which are needed to describe dynamical correlation or electronic screening. Regional embedding is also similar to the subsystem projected AO decomposition approach.^{36,37}

We define an operator \hat{P}_A that project onto some atomic orbitals (AOs) μ, ν of a user-selected set of atoms $\{A\}$,

$$\hat{P}_A = \sum_{\mu\nu \in \{A\}} |\mu\rangle [\mathbf{S}]_{\mu\nu}^{-1} \langle \nu|, \quad (1)$$

where \mathbf{S} is the overlap matrix. In regional embedding, the occupied orbitals are projected onto a minimal set of AOs centered on the atoms in $\{A\}$, and the virtual orbitals are projected onto the full set of computational AOs centered on the atoms in $\{A\}$. The active space is defined via the eigenvectors of the respective projection operators (which are rotation matrices of the canonical occupied and unoccupied orbitals) with

eigenvalues above a cutoff. Definition of the active space thus requires specification of the atoms to be included in the projection operator and an eigenvalue cutoff (or equivalently a number of occupied and unoccupied orbitals to keep). Here we use an eigenvalue cutoff of 0.1 in all results, which generates unoccupied orbitals spaces that are significantly larger than the occupied orbital spaces because of their projections onto different sets of AOs. In the definition of the projection operator, we include all atoms inside a sphere centered on the defect, and we grow the active space by increasing the radius of this sphere. We will henceforth refer to the active space identified in this manner as a “local” active space.

C. Natural transition orbitals

Our third and final active space choice is motivated by the successful use of approximate natural orbitals in ground state calculations. For excited state calculations, the analogue is the use of approximate natural transition orbitals (NTOs),³⁸ which have been previously used to reduce the cost of CC calculations of molecular excited states.^{39–43} NTOs are defined via the left and right singular vectors of the transition density matrix $\rho_{pq}^{(n)} = \langle \Psi_0 | a_q^\dagger a_p | \Psi_n \rangle$, where $\Psi_{0/n}$ are the ground and excited states. When the electronic structure does not require a multireference description, configuration interaction with single excitations (CIS) provides an economical route to approximate NTOs, which is the approach we use here. Specifically, the occupied NTO rotation matrix \mathbf{U} and unoccupied NTO rotation matrix \mathbf{V} are obtained from the singular value decomposition

$$\mathbf{C} = \mathbf{U} \boldsymbol{\sigma} \mathbf{V}^T \quad (2)$$

where $|\Psi_n\rangle = \sum_{ai} C_i^a a_a^\dagger a_i |\Phi_0\rangle$ is the CIS wavefunction of the full supercell with all orbitals. The NTO active space is made of pairs of orbitals from \mathbf{U} and \mathbf{V} with the largest singular values σ . Definition of the NTO active space requires a singular value cutoff (or a number of occupied/unoccupied orbitals to keep). Because the occupied and unoccupied orbitals are added in pairs, after exhaustion of the occupied orbital space, we canonicalize the remaining unoccupied orbitals and add them in order of increasing energy.

D. Correcting for active space size

As discussed in Sec. I, quantum embedding results can be improved by approximately correcting for the finite size of the active space. Instead of downfolding external excitations into the Hamiltonian, e.g., via the cRPA, we test the performance of a simple composite correction. Specifically, we correct the CCSD excitation energy at the CIS level,

$$E_{\text{CCSD}}^{\text{full}} \approx E_{\text{CCSD}}^{\text{act}} + \delta, \quad (3a)$$

$$\delta = E_{\text{CIS}}^{\text{full}} - E_{\text{CIS}}^{\text{act}}, \quad (3b)$$

where “full” and “act” indicate calculations on the full system and in the active space. This correction is affordable due to the

low cost of CIS (comparable to that of the underlying HF calculation), and it is essentially free when using the NTO active space. For comparison with our uncorrected CCSD results, the convergence of the CIS excitation energy in the above three active spaces is shown in the App. A. We note that CIS and RPA are similar theories, and a comparison between composite corrections and downfolding would be interesting for future work. Other lower-cost methods can also be used for the calculation of NTOs or for the composite correction, such as CC2, partitioned equation-of-motion MP2, or CIS(D).⁴⁴

III. RESULTS

We compare the above three active space choices for three representative, electrically neutral point defects: a $C_B C_N$ carbon dimer defect in two-dimensional hexagonal boron nitride (hBN), an O_V oxygen vacancy in three-dimensional rock salt MgO (the so-called *F*-center), and a C_V carbon vacancy in three-dimensional carbon diamond (the so-called GR1 defect). Geometry optimizations were performed with Quantum Espresso⁴⁵ using density functional theory (DFT), the PBE functional,⁴⁶ and Kresse-Joubert projector-augmented wave pseudopotentials.⁴⁷ For $C_B C_N$ in hBN, we used a kinetic energy cutoff of 70 Ry and a $4 \times 4 \times 4$ k -point mesh; for O_V in MgO, we used a kinetic cutoff of 70 Ry and a $9 \times 9 \times 9$ k -point mesh; and for C_V in diamond, we used a kinetic energy cutoff of 60 Ry and a $6 \times 6 \times 6$ k -point mesh.

CIS and CCSD electronic structure calculations were performed at the Γ point with PySCF,^{48–50} using periodic Gaussian density fitting.^{51,52} We employed GTH pseudopotentials⁵³ optimized for HF theory⁵⁴ ([He] core for all atoms) and associated correlation-consistent double-zeta Gaussian basis sets optimized for solids (GTH-cc-pVDZ).⁵⁵ For vacancy defects, we use a ghost atom with the same basis functions as the missing atom. Although we have not exhaustively quantified errors due to the double-zeta basis, preliminary calculations suggest that these errors are on the 0.1 eV order of magnitude. All studied defects have closed-shell, spin-singlet ground states and, for simplicity, we only study spin-singlet excitations. Spin-triplet excitations can be straightforwardly studied using the same methods, and these are especially interesting in the context of qubit realization.

A. $C_B C_N$ in hBN

Our first example is the $C_B C_N$ carbon dimer in hBN. We study an $8 \times 8 \times 1$ primitive supercell containing 128 atoms with 20 Å of perpendicular vacuum (which converges the excitation energies). With our employed basis set and pseudopotentials, the supercell has 1,664 total orbitals (256 occupied, 1,408 unoccupied), which is slightly beyond the reach of a routine CCSD calculation. The canonical valence orbital energies are shown in Fig. 1(a). The in-gap defect orbitals are indicated in red and plotted over the atomic structure in Fig. 1(b), and they can be seen to be reasonably localized to the defect region. The HF defect orbital gap is 11.32 eV and our best es-

timate of the CCSD excitation energy (obtained as described below) is 4.76 eV.

In Fig. 1(b), we show the lowest-lying CCSD excitation energy as a function of the total number of orbitals (occupied plus unoccupied) in the three active spaces defined in Sec. II. The excitation energy converges fastest in the NTO active space, followed by the local (regional embedding) active space, followed by the canonical active space. In the NTO active space, the excitation energy is converged to 0.2 eV using about 500 orbitals. The good performance of the NTO active space indicates that the CIS wavefunction provides a semiquantitative description of the transition density matrix. For small active spaces, the local active space yields excitations that are much too high. However, it performs well for active spaces with more than about 400 orbitals, giving a result in good agreement with the NTO active space. The canonical orbital active space is very poor and the results converge extremely slowly, which is a well-known behavior of wavefunction-based dynamical correlation.

The CIS composite correction improves the convergence of all methods, but in qualitatively different ways. Because the NTO basis is almost perfect for CIS (by construction), the

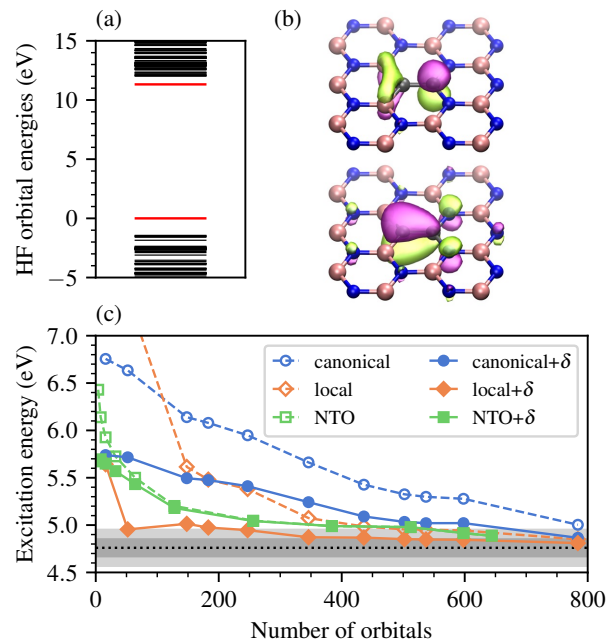


FIG. 1. Results for the $C_B C_N$ substitutional defect in a $8 \times 8 \times 1$ supercell of hBN. (a) The Hartree-Fock molecular orbital energies near the band gap. Red lines indicate the highest occupied and lowest unoccupied defect orbitals. (b) The lowest occupied (top) and highest occupied (bottom) canonical HF defect orbitals; only atoms near the defect are shown. (c) The CCSD excitation energy as a function of active space size for canonical, local (regional embedding), and CIS NTO active spaces (dashed lines with open symbols). Also shown are the results with a composite correction δ from a CIS calculation of the full supercell (solid lines with filled symbols). Dotted line indicates our best estimate via M^{-1} extrapolation and gray bars are ± 0.1 eV and ± 0.2 eV windows.

TABLE I. First singlet excitation energy of the $C_B C_N$ defect in hexagonal boron nitride.

Method	Structure	Exc. energy (eV)
CCSD (this work)	periodic	4.76
TDDFT@CAM-B3LYP ⁵⁶	cluster	4.78
Δ SCF@HSE($\alpha = 0.4$) ⁵⁷	periodic	4.53
TDDFT@PBE0 ⁵⁸	cluster	4.61
evGW+BSE@PBE0 ⁵⁸	cluster	4.64
cRPA+ED(2e,2o)@PBE ¹⁷	periodic	3.98
cRPA+ED(2e,2o)@HSE($\alpha = 0.4$) ¹⁷	periodic	4.23
Experiment (ZPL) ^{59,60}	—	4.1
Experiment (est. vertical) ⁵⁸	—	4.6

CIS composite correction in a truncated NTO active space is very small and does not significantly impact the CCSD results. In contrast, the CIS composite correction to the local active space is significant and provides good performance: the corrected excitation energy is accurate to 0.2 eV using only 52 orbitals! The composite correction to results in the canonical active space reduces the magnitude of the error but does not significantly change the rate of convergence.

To estimate the full supercell limit, we extrapolate our composite-corrected result in the local active space assuming M^{-1} convergence, where M is the number of basis functions. This yields a vertical excitation energy of 4.76 eV; analogous extrapolation of results in alternative active spaces gives similar results, differing by less than 0.1 eV. In Tab. I, we compare this value to previously obtained vertical excitation energies using TDDFT with the CAMB3LYP⁵⁶ and PBE0⁵⁸ functionals, Δ SCF with the HSE functional,⁵⁷ eigenvalue self-consistent GW approximation and Bethe-Salpeter equation (BSE) started from PBE0,⁵⁸ and constrained random-phase approximation (cRPA) screening combined with exact diagonalization (ED) in a minimal active space of two electrons in two orbitals (2e,2o);¹⁷ these cRPA+ED results were obtained with both PBE and HSE and include double-counting corrections that mitigate the dependence on this starting point. In both of the Δ SCF and cRPA+ED calculations, HSE calculations were performed with the modified exact-exchange fraction $\alpha = 0.4$. The table indicates whether a finite cluster or periodic structure were used to model the crystal.

We see that our CCSD prediction is within 0.1–0.2 eV of Δ SCF, TDDFT, and GW+BSE results, and about 0.6–0.8 eV higher in energy than cRPA+ED results. We propose that this system is not especially correlated and does not require the multiconfigurational treatment of ED; instead, dynamical correlation is important—as evidenced by the large number of orbitals required and slow convergence—and cRPA only captures this dynamical correlation approximately.

Bulk hBN exhibits a zero-phonon line (ZPL) around 4.1 eV^{59,60} that has been attributed to the optical absorption of the $C_B C_N$ dimer defect,⁵⁷ although we emphasize that this assignment is not definite. For direct comparison, lattice reorganization energies, zero-point vibrational energies, and inter-layer or substrate screening effects need to be accounted for. Previous work has estimated the first two corrections lower the vertical excitation energy by about 0.2–0.3 eV^{57,58} and

the screening correction lowers it by another 0.3 eV.⁵⁸ In this light, our prediction of 4.76 eV might be an overestimation of only about 0.2 eV, which is typical for CCSD.

B. O_V in MgO

Our next example is the O_V oxygen vacancy in MgO, also known as a neutral F -center. For reference, previous work from our group used periodic CCSD to estimate the excitation energy of non-defective MgO and found 8.3 eV,²⁷ which can be compared to the experimental value of 7.6.⁶¹ Electron-phonon calculations predict a zero-point renormalization of the band gap by 0.3–0.6 eV,^{62–64} suggesting that CCSD overestimates the vertical electronic excitation energy by 0.1–0.4 eV.

We study a $3 \times 3 \times 3$ conventional supercell containing 215 atoms and one oxygen ghost atom. With our basis set and pseudopotentials, the supercell has 2,916 orbitals (861 occupied and 2,055 unoccupied), which is much too big for a conventional CCSD calculation. The HF molecular orbital energies and defect orbitals are plotted in Figs. 2(a) and (b), where now the lowest-lying unoccupied defect orbitals (threefold degenerate) are not in the band gap of the crystal. Moreover, this defect orbital is three-fold degenerate due to its p -type symmetry, and the excitations energies are analogously degenerate. The HF defect gap is 11.33 eV and our best estimate of the CCSD excitation energy is 5.31 eV.

In Fig. 2(b), we plot the CCSD excitation energy in the same three active space types, without and with CIS com-

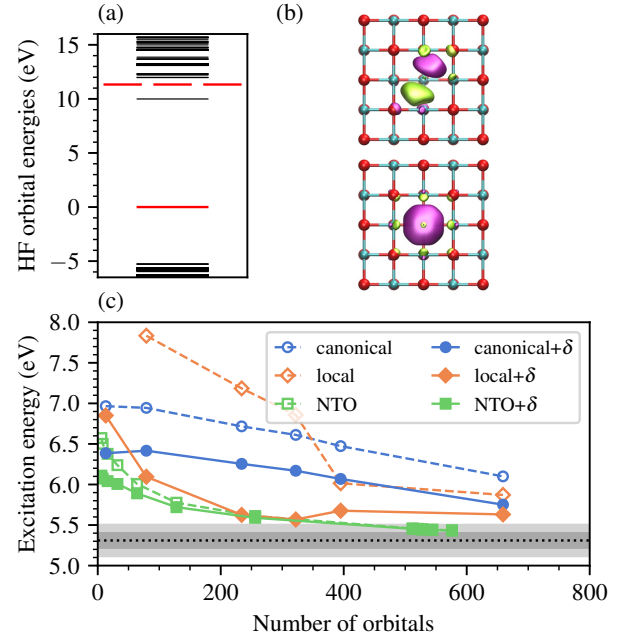


FIG. 2. The same as Fig. 1, but for the O_V oxygen vacancy (F -center) in a $3 \times 3 \times 3$ supercell of MgO containing 215 atoms. Only one of the three degenerate lowest unoccupied defect orbitals is shown.

TABLE II. First singlet excitation energy of the O_V (F -center) defect in MgO.

Method	Structure	Exc. energy (eV)
CCSD (this work)	periodic	5.31
CASPT2 (2e,2o) ⁶⁵	cluster	5.44
G_0W_0 +BSE@LDA0 ⁶²	periodic	4.95
DMC ⁶⁶	periodic	5.0 ± 0.1
CCSD ¹²	periodic	5.28
Experiment (est. vertical) ⁶⁷⁻⁶⁹	—	5.0

posite corrections. Unlike for $C_B C_N$, the dimensionality of the MgO crystal prevents us from achieving converged agreement between various active space choices. Results in the NTO active space converge the fastest, and composite corrections are small, but complete convergence is not observed. Extrapolation of the composite-corrected NTO results assuming M^{-1} convergence yields our best prediction of 5.31 eV (again, analogous extrapolation of canonical orbital results gives good agreement). The uncorrected local orbital results show a plateau at the two largest active spaces. The same feature is also seen in the CIS calculation (see App. A), which requires over 1000 orbitals for convergence. Although the qualitative similarity explains the relatively good performance of the composite correction, the cancellation is imperfect and so convergence is not observed in the corrected local-orbital CCSD calculations.

In Tab. II, we compare our singlet excitation energy to that calculated by complete active space self-consistent field plus second-order perturbation theory (CASPT2),⁶⁵ G_0W_0 +BSE,⁶² diffusion Monte Carlo (DMC),⁶⁶ and CCSD.¹² The CASPT2 calculations were done with a 26-atom cluster model containing the oxygen vacancy and three shells (14 Mg atoms and 12 O atoms), surrounded by ab initio model potentials and an array of optimized point charges; a minimal active space of two electrons in two orbitals (2e,2o) was used, and increases to the active space size increased the excitation energy by about 0.05 eV. The G_0W_0 +BSE calculations were performed on top of a LDA reference with a one-shot correction to include 25% exact exchange (termed LDA0 in Ref. 62). The DMC calculations used the fixed-node approximation with a DFT-based Slater-Jastrow trial wavefunction and supercells containing up to 64 atoms. Finally, the CCSD calculations,¹² which are most directly comparable to our own, were performed for several supercell sizes and basis set truncations and then extrapolated. For comparison, the largest supercell studied contained 127 atoms (compared to our 215 atoms) and a canonical orbital active space was used containing up to about 701 orbitals (comparable to our own), although orbital character was considered in the construction of the active space. Our CCSD results and the extrapolated CCSD results from Ref. 12 agree almost perfectly (0.03 eV difference), and both are within about 0.15 eV of the CASPT2 results.⁶⁵

This agreement between different calculations and different methods is encouraging. Experimental optical measurements exhibit a broad absorption band with a maximum around

5.0 eV, which has been assigned to the neutral F -center.^{67,68} Vibronic modeling⁶⁹ suggests a ZPL at about 4.0 eV and a reorganization energy of about 1.0 eV (i.e., a very large Huang-Rhys factor of about 30, which is consistent with the broad absorption band); therefore, the peak location of 5.0 eV is a reasonable estimation of the true vertical excitation energy. The remaining 0.3 eV discrepancy between CCSD and experimental measurements is typical of CCSD and consistent with its accuracy for non-defective MgO.

C. C_V in diamond

Our final example is the C_V carbon vacancy in diamond. This particular system is a valuable prototype of diamond defects, such as the popular negatively charged nitrogen vacancy center.⁷⁰ Again for reference, periodic CCSD predicts an excitation of 7.47 eV for non-defective diamond, which can be compared to the experimental value of 7.3 eV.⁷¹ Electron-phonon calculations predict a zero-point renormalization of the band gap by 0.3 eV,⁶⁴ suggesting that CCSD underestimates the excitation energy by about 0.1 eV.

For the C_V vacancy, we study a $2 \times 2 \times 2$ body-centered cubic supercell containing 255 carbon atoms and one carbon ghost atom. With our employed basis set and pseudopotentials, the system has 3,328 orbitals (510 occupied and 2,818 unoccupied orbitals), which is our largest system studied and impossible to treat with conventional CCSD. The HF defect gap is 6.63 eV and our best estimate of the CCSD excitation energy is 2.09 eV. Before presenting our results, we first ad-

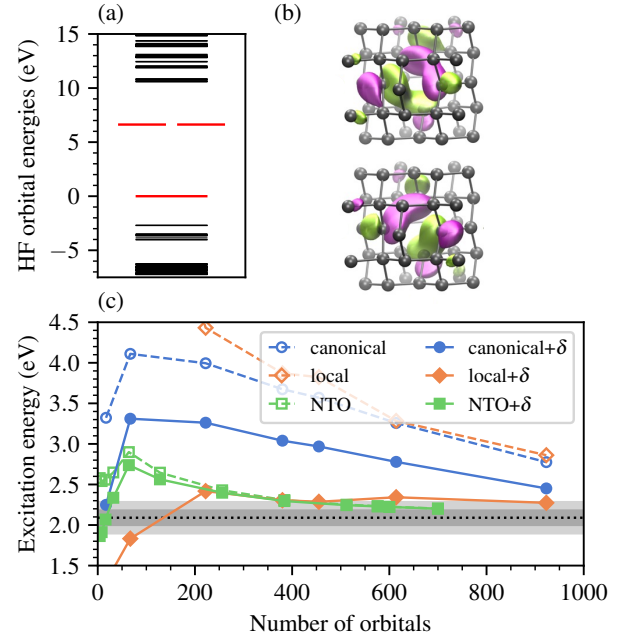


FIG. 3. The same as Fig. 1, but for the C_V carbon vacancy (GR1 defect) in a $2 \times 2 \times 2$ BCC supercell of diamond containing 255 atoms. Only one of the two degenerate lowest unoccupied defect orbitals is shown.

TABLE III. First singlet excitation energies of the C_V (GR1) defect in diamond.

Method	Structure	Exc. energy (eV)
CCSD (this work)	periodic / D_{2d}	2.09
DMC ⁷²	periodic / T_d	1.51 ± 0.34
Δ SCF@B3LYP ⁷⁶	periodic / pseudo- T_d	1.57
Experiment (ZPL) ⁷⁷	—	1.67
Experiment (est. vertical) ⁷⁸	—	2.2

dress the nuclear geometry and associated electronic structure.

Removing a carbon atom from diamond yields a structure with T_d symmetry and an open shell due to the placement of two valence electrons into a threefold degenerate set of orbitals with t_2 symmetry. This valence suggests a multiplet structure of low-lying many-body states with multi-configurational character, which has been studied by fixed-node DMC with a symmetry-adapted multi-Slater-Jastrow trial wavefunction.⁷² Alternatively, coupling to the lattice can induce a Jahn-Teller distortion^{73,74} that lowers the symmetry to D_{2d} , breaks the threefold degenerate t_2 orbitals into one lower a orbital and two higher e orbitals, and thus yields a closed-shell ground-state singlet configuration. While this latter scenario is at odds with experimental support for tetrahedral symmetry at the vacancy,⁷³ a quantum *dynamic* Jahn-Teller mechanism is largely supported and has been studied by anharmonic vibrational calculations.⁷⁵

Because CC theory is only appropriate for single-reference ground states, we focus on the statically distorted D_{2d} structure, which constitutes one of the points on the Born-Oppenheimer ground-state surface that is needed to define the anharmonic vibrational problem. At the HF level, the orbital energies and defect orbitals are shown in Figs. 3(a) and (b). The orbital energies are inside the band gap of diamond and the lowest-lying unoccupied defect orbital is two-fold degenerate.

The convergence of the CCSD excitation energy is shown in Fig. 3(c). Results obtained with the canonical active space converge smoothly but slowly, and, as before, composite corrections decrease the magnitude of the error but do not increase the rate of convergence. Uncorrected results in the local orbital active space converge the slowest, but the composite correction is excellent and yields good predictions using only 200–400 orbitals. The NTO results are arguably the best, both without and with composite corrections. Unlike for O_V in MgO, the excitation energy of C_V in diamond converges sufficiently quickly that we can achieve agreement between different active space choices using as few as about 380 orbitals or 10% of the total number of orbitals! Using M^{-1} extrapolation of the corrected NTO results, our best estimate of the CCSD excitation energy is 2.09 eV.

In Tab. III, we compare our prediction to the multiconfigurational DMC results in T_d geometry and to very recent Δ SCF@B3LYP results in a pseudo- T_d geometry (only slight symmetry breaking); the latter breaks spin symmetry in order to stabilize a single configuration ground state. The CCSD excitation energy is 0.5–0.6 eV higher than that of these other

calculations. Experimental low-temperature spectra show a zero-phonon line at 1.67 eV,⁷⁷ which has been assigned to the C_V (GR1) vacancy. Vibronic modeling of the statically distorted Jahn-Teller structure predicts a lattice reorganization energy of about 0.5 eV,⁷⁸ suggesting a true vertical excitation energy of about 2.2 eV. The CCSD prediction is therefore in excellent agreement and, interestingly, an underestimation, which is the same as in non-defective diamond.

IV. CONCLUSION

To summarize, we have explored the slow convergence of excitation energies of defects in solids with respect to the number of orbitals using CCSD as a high-level method. In the context of active-space based quantum embedding, we studied two alternatives to canonical orbitals—local orbitals and natural transition orbitals—which expedite the convergence, especially when using composite corrections. Although achieving precision to better than 0.1 eV still requires extrapolation, the uncertainty introduced by extrapolation is significantly reduced. For the three defects studied, we find that CCSD predicts vertical excitation energies that are accurate to 0.1–0.3 eV when compared to putative experimental values as long as vibrational corrections are accounted for.

We expect the methods introduced here to be applicable to other single-reference electronic structure methods, such as GW-BSE. Future work could aim to enforce self-consistency between the low-level and high-level treatments of the embedded system, as an improvement to the one-shot embedding used here. Extension to defects with multiconfigurational ground states requires further consideration, both with respect to the active space selection and the challenge of growing the active space. A similar study of existing methods, such as cRPA+ED, would be an interesting first step, including the performance of alternative active spaces and the quantitative treatment of dynamical correlation by the cRPA.

ACKNOWLEDGMENTS

We thank Cyrus Dreyer, Xiao Wang, Hong-Zhou Ye, and Shiwei Zhang for helpful discussions. This work was supported in part by the US Air Force Office of Scientific Research under Grant No. FA9550-21-1-0400. The Flatiron Institute is a division of the Simons Foundation.

Appendix A: CIS excitation energy convergence

In Fig. 4, we present the CIS excitation energy of the three defects studied in the main text.

REFERENCES

- ¹F. Jelezko and J. Wrachtrup, “Single defect centres in diamond: A review,” *Phys. Status Solidi A* **203**, 3207–3225 (2006).

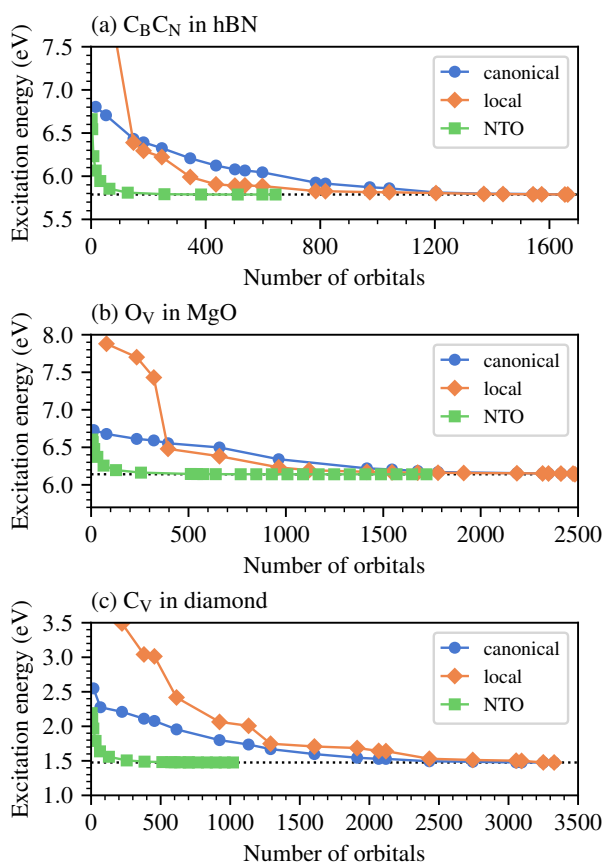


FIG. 4. CIS excitation energy of the three defects studied in the main text (indicated in each panel) using the three active space choices (indicated in the legend). The final data point of the canonical and local results corresponds to the full supercell limit in the employed basis. For visual clarity, NTO results are not shown for large number of orbitals.

- ²J. R. Weber, W. F. Koehl, J. B. Varley, A. Janotti, B. B. Buckley, C. G. V. de Walle, and D. D. Awschalom, "Quantum computing with defects," *Proc. Natl. Acad. Sci.* **107**, 8513–8518 (2010).
- ³T. T. Tran, C. Elbadawi, D. Totonjian, C. J. Lobo, G. Grosso, H. Moon, D. R. Englund, M. J. Ford, I. Aharonovich, and M. Toth, "Robust multicolor single photon emission from point defects in hexagonal boron nitride," *ACS Nano* **10**, 7331–7338 (2016).
- ⁴N. D. M. Hine, K. Frensch, W. M. C. Foulkes, and M. W. Finnis, "Supercell size scaling of density functional theory formation energies of charged defects," *Phys. Rev. B* **79**, 024112 (2009).
- ⁵C. Freysoldt, J. Neugebauer, and C. G. V. de Walle, "Fully ab initio finite-size corrections for charged-defect supercell calculations," *Phys. Rev. Lett.* **102**, 016402 (2009).
- ⁶C. Freysoldt, B. Grabowski, T. Hickel, J. Neugebauer, G. Kresse, A. Janotti, and C. G. V. de Walle, "First-principles calculations for point defects in solids," *Rev. Mod. Phys.* **86**, 253–305 (2014).
- ⁷Á. Gali, "Ab initio theory of the nitrogen-vacancy center in diamond," *Nanophotonics* **8**, 1907–1943 (2019).
- ⁸D. Erbetta, D. Ricci, and G. Pacchioni, "Simplified embedding schemes for the quantum-chemical description of neutral and charged point defects in SiO_2 and related dielectrics," *J. Chem. Phys.* **113**, 10744–10752 (2000).
- ⁹D. V. Chulhai and J. D. Goodpaster, "Projection-based correlated wave function in density functional theory embedding for periodic systems," *J. Chem. Theory Comput.* **14**, 1928–1942 (2018).

- ¹⁰B. Eskridge, H. Krakauer, and S. Zhang, "Local embedding and effective downfolding in the auxiliary-field quantum Monte Carlo method," *J. Chem. Theory Comput.* **15**, 3949–3959 (2019).
- ¹¹J. R. Reimers, J. Shen, M. Kianinia, C. Bradac, I. Aharonovich, M. J. Ford, and P. Piecuch, "Photoluminescence, photophysics, and photochemistry of the V_B^- defect in hexagonal boron nitride," *Phys. Rev. B* **102**, 144105 (2020).
- ¹²A. Gallo, F. Hummel, A. Imler, and A. Grüneis, "A periodic equation-of-motion coupled-cluster implementation applied to F -centers in alkaline earth oxides," *J. Chem. Phys.* **154**, 064106 (2021).
- ¹³T. Schäfer, F. Libisch, G. Kresse, and A. Grüneis, "Local embedding of coupled cluster theory into the random phase approximation using plane waves," *J. Chem. Phys.* **154**, 011101 (2021).
- ¹⁴B. T. G. Lau, G. Knizia, and T. C. Berkelbach, "Regional embedding enables high-level quantum chemistry for surface science," *J. Phys. Chem. Lett.* **12**, 1104–1109 (2021).
- ¹⁵H. Ma, N. Sheng, M. Govoni, and G. Galli, "Quantum embedding theory for strongly correlated states in materials," *J. Chem. Theory Comput.* **17**, 2116–2125 (2021).
- ¹⁶A. Mitra, H. Q. Pham, R. Pandharkar, M. R. Hermes, and L. Gagliardi, "Excited states of crystalline point defects with multireference density matrix embedding theory," *J. Phys. Chem. Lett.* **12**, 11688–11694 (2021).
- ¹⁷L. Muechler, D. I. Badrtdinov, A. Hampel, J. Cano, M. Rösner, and C. E. Dreyer, "Quantum embedding methods for correlated excited states of point defects: Case studies and challenges," *Phys. Rev. B* **105**, 235104 (2022).
- ¹⁸T. Klüner, N. Govind, Y. A. Wang, and E. A. Carter, "Periodic density functional embedding theory for complete active space self-consistent field and configuration interaction calculations: Ground and excited states," *J. Chem. Phys.* **116**, 42 (2002).
- ¹⁹Y. G. Khait and M. R. Hoffmann, "Embedding theory for excited states," *J. Chem. Phys.* **133**, 044107 (2010).
- ²⁰N. H. List, J. M. H. Olsen, and J. Kongsted, "Excited states in large molecular systems through polarizable embedding," *Phys. Chem. Chem. Phys.* **18**, 20234–20250 (2016).
- ²¹X. Wen, D. S. Graham, D. V. Chulhai, and J. D. Goodpaster, "Absolutely localized projection-based embedding for excited states," *J. Chem. Theory Comput.* **16**, 385–398 (2019).
- ²²H. K. Tran, T. V. Voorhis, and A. J. W. Thom, "Using SCF metadynamics to extend density matrix embedding theory to excited states," *J. Chem. Phys.* **151**, 034112 (2019).
- ²³H.-Z. Ye, H. K. Tran, and T. V. Voorhis, "Accurate electronic excitation energies in full-valence active space via bootstrap embedding," *J. Chem. Theory Comput.* **17**, 3335–3347 (2021).
- ²⁴F. Aryasetiawan, M. Imada, A. Georges, G. Kotliar, S. Biermann, and A. I. Lichtenstein, "Frequency-dependent local interactions and low-energy effective models from electronic structure calculations," *Phys. Rev. B* **70**, 195104 (2004).
- ²⁵J. F. Stanton and R. J. Bartlett, "The equation of motion coupled-cluster method. A systematic biorthogonal approach to molecular excitation energies, transition probabilities, and excited state properties," *J. Chem. Phys.* **98**, 7029–7039 (1993).
- ²⁶A. I. Krylov, "Equation-of-motion coupled-cluster methods for open-shell and electronically excited species: The hitchhiker's guide to fock space," *Annu. Rev. Phys. Chem.* **59**, 433–462 (2008).
- ²⁷X. Wang and T. C. Berkelbach, "Excitons in solids from periodic equation-of-motion coupled-cluster theory," *J. Chem. Theory Comput.* **16**, 3095–3103 (2020).
- ²⁸X. Wang and T. C. Berkelbach, "Absorption spectra of solids from periodic equation-of-motion coupled-cluster theory," *J. Chem. Theory Comput.* **17**, 6387–6394 (2021).
- ²⁹K. Kowalski, "Properties of coupled-cluster equations originating in excitation sub-algebras," *J. Chem. Phys.* **148**, 094104 (2018).
- ³⁰J. M. Callahan, M. F. Lange, and T. C. Berkelbach, "Dynamical correlation energy of metals in large basis sets from downfolding and composite approaches," *J. Chem. Phys.* **154**, 211105 (2021).
- ³¹T. Zhu and G. K.-L. Chan, "Ab initio full cell GW + DMFT for correlated materials," *Phys. Rev. X* **11**, 021006 (2021).
- ³²N. Marzari, A. A. Mostofi, J. R. Yates, I. Souza, and D. Vanderbilt, "Maximally localized Wannier functions: Theory and applications," *Rev. Mod. Phys.* **84**, 1419–1475 (2012).

- ³³G. Knizia and G. K.-L. Chan, “Density matrix embedding: A simple alternative to dynamical mean-field theory,” *Phys. Rev. Lett.* **109**, 186404 (2012).
- ³⁴B.-X. Zheng and G. K.-L. Chan, “Ground-state phase diagram of the square lattice Hubbard model from density matrix embedding theory,” *Phys. Rev. B* **93**, 035126 (2016).
- ³⁵E. R. Sayfutyarova, Q. Sun, G. K.-L. Chan, and G. Knizia, “Automated construction of molecular active spaces from atomic valence orbitals,” *J. Chem. Theory Comput.* **13**, 4063–4078 (2017).
- ³⁶D. Claudino and N. J. Mayhall, “Automatic partition of orbital spaces based on singular value decomposition in the context of embedding theories,” *J. Chem. Theory Comput.* **15**, 1053–1064 (2019).
- ³⁷D. Claudino and N. J. Mayhall, “Simple and efficient truncation of virtual spaces in embedded wave functions via concentric localization,” *J. Chem. Theory Comput.* **15**, 6085–6096 (2019).
- ³⁸R. L. Martin, “Natural transition orbitals,” *J. Chem. Phys.* **118**, 4775–4777 (2003).
- ³⁹R. A. Mata and H. Stoll, “An incremental correlation approach to excited state energies based on natural transition/localized orbitals,” *J. Chem. Phys.* **134**, 034122 (2011).
- ⁴⁰B. Helmich and C. Hättig, “Local pair natural orbitals for excited states,” *J. Chem. Phys.* **135**, 214106 (2011).
- ⁴¹P. Baudin and K. Kristensen, “Correlated natural transition orbital framework for low-scaling excitation energy calculations (CorNFlEx),” *J. Chem. Phys.* **146**, 214114 (2017).
- ⁴²A. K. Dutta, M. Nooijen, F. Neese, and R. Izsák, “Automatic active space selection for the similarity transformed equations of motion coupled cluster method,” *J. Chem. Phys.* **146**, 074103 (2017).
- ⁴³Y. C. Park, A. Perera, and R. J. Bartlett, “Low scaling EOM-CCSD and EOM-MBPT(2) method with natural transition orbitals,” *J. Chem. Phys.* **149**, 184103 (2018).
- ⁴⁴J. J. Goings, M. Caricato, M. J. Frisch, and X. Li, “Assessment of low-scaling approximations to the equation of motion coupled-cluster singles and doubles equations,” *J. Chem. Phys.* **141**, 164116 (2014).
- ⁴⁵P. Giannozzi, S. Baroni, N. Bonini, M. Calandra, R. Car, C. Cavazzoni, D. Ceresoli, G. L. Chiarotti, M. Cococcioni, I. Dabo, A. D. Corso, S. de Gironcoli, S. Fabris, G. Fratesi, R. Gebauer, U. Gerstmann, C. Gougousis, A. Kokalj, M. Lazzeri, L. Martin-Samos, N. Marzari, F. Mauri, R. Mazzarello, S. Paolini, A. Pasquarello, L. Paulatto, C. Sbraccia, S. Scandolo, G. Sclauzero, A. P. Seitsonen, A. Smogunov, P. Umari, and R. M. Wentzcovitch, “QUANTUM ESPRESSO: a modular and open-source software project for quantum simulations of materials,” *J. Phys.: Condens. Matter* **21**, 395502 (2009).
- ⁴⁶J. P. Perdew, K. Burke, and M. Ernzerhof, “Generalized gradient approximation made simple,” *Phys. Rev. Lett.* **77**, 3865–3868 (1996).
- ⁴⁷G. Kresse and D. Joubert, “From ultrasoft pseudopotentials to the projector augmented-wave method,” *Phys. Rev. B* **59**, 1758–1775 (1999).
- ⁴⁸Q. Sun, T. C. Berkelbach, N. S. Blunt, G. H. Booth, S. Guo, Z. Li, J. Liu, J. D. McClain, E. R. Sayfutyarova, S. Sharma, S. Wouters, and G. K.-L. Chan, “PySCF: The Python-based simulations of chemistry framework,” *WIREs Comput. Mol. Sci.* **8** (2017), 10.1002/wcms.1340.
- ⁴⁹Q. Sun, X. Zhang, S. Banerjee, P. Bao, M. Barbry, N. S. Blunt, N. A. Bogdanov, G. H. Booth, J. Chen, Z.-H. Cui, J. J. Eriksen, Y. Gao, S. Guo, J. Hermann, M. R. Hermes, K. Koh, P. Koval, S. Lehtola, Z. Li, J. Liu, N. Mardirossian, J. D. McClain, M. Motta, B. Mussard, H. Q. Pham, A. Pulkin, W. Purwanto, P. J. Robinson, E. Ronca, E. R. Sayfutyarova, M. Scheurer, H. F. Schurkus, J. E. T. Smith, C. Sun, S.-N. Sun, S. Upadhyay, L. K. Wagner, X. Wang, A. White, J. D. Whitfield, M. J. Williamson, S. Wouters, J. Yang, J. M. Yu, T. Zhu, T. C. Berkelbach, S. Sharma, A. Y. Sokolov, and G. K.-L. Chan, “Recent developments in the PySCF program package,” *J. Chem. Phys.* **153**, 024109 (2020).
- ⁵⁰J. McClain, Q. Sun, G. K.-L. Chan, and T. C. Berkelbach, “Gaussian-based coupled-cluster theory for the ground-state and band structure of solids,” *J. Chem. Theory Comput.* **13**, 1209–1218 (2017).
- ⁵¹H.-Z. Ye and T. C. Berkelbach, “Fast periodic Gaussian density fitting by range separation,” *J. Chem. Phys.* **154**, 131104 (2021).
- ⁵²H.-Z. Ye and T. C. Berkelbach, “Tight distance-dependent estimators for screening two-center and three-center short-range Coulomb integrals over Gaussian basis functions,” *J. Chem. Phys.* **155**, 124106 (2021).
- ⁵³S. Goedecker, M. Teter, and J. Hutter, “Separable dual-space Gaussian pseudopotentials,” *Phys. Rev. B* **54**, 1703–1710 (1996).
- ⁵⁴J. Hutter, “New optimization of gth pseudopotentials for pbe, scan, pbe0 functionals, gth pseudopotentials for hartree-fock, nlcc pseudopotentials for pbe,” <https://github.com/juerghutter/GTH> (2019).
- ⁵⁵H.-Z. Ye and T. C. Berkelbach, “Correlation-consistent Gaussian basis sets for solids made simple,” *J. Chem. Theory Comput.* **18**, 1595–1606 (2022).
- ⁵⁶T. Korona and M. Chojacki, “Exploring point defects in hexagonal boron-nitrogen monolayers,” *Int. J. Quantum Chem.* **119**, e25925 (2019).
- ⁵⁷M. Mackoito-Sinkevičienė, M. Maciaszek, C. G. V. de Walle, and A. Alkauskas, “Carbon dimer defect as a source of the 4.1 eV luminescence in hexagonal boron nitride,” *Appl. Phys. Lett.* **115**, 212101 (2019).
- ⁵⁸M. Winter, M. H. E. Bousquet, D. Jacquemin, I. Duchemin, and X. Blase, “Photoluminescent properties of the carbon-dimer defect in hexagonal boron-nitride: A many-body finite-size cluster approach,” *Phys. Rev. Materials* **5**, 095201 (2021).
- ⁵⁹L. Museur, E. Feldbach, and A. Kanaev, “Defect-related photoluminescence of hexagonal boron nitride,” *Phys. Rev. B* **78**, 155204 (2008).
- ⁶⁰X. Z. Du, J. Li, J. Y. Lin, and H. X. Jiang, “The origin of deep-level impurity transitions in hexagonal boron nitride,” *Appl. Phys. Lett.* **106**, 021110 (2015).
- ⁶¹D. M. Roessler and W. C. Walker, “Optical constants of magnesium oxide and lithium fluoride in the far ultraviolet,” *J. Opt. Soc. Am.* **57**, 835 (1967).
- ⁶²P. Rinke, A. Schleife, E. Kioupakis, A. Janotti, C. Rödl, F. Bechstedt, M. Scheffler, and C. G. V. de Walle, “First-principles optical spectra for *F* centers in MgO,” *Phys. Rev. Lett.* **108**, 126404 (2012).
- ⁶³G. Antonius, S. Poncé, E. Lantagne-Hurtubise, G. Auclair, X. Gonze, and M. Côté, “Dynamical and anharmonic effects on the electron-phonon coupling and the zero-point renormalization of the electronic structure,” *Phys. Rev. B* **92**, 085137 (2015).
- ⁶⁴A. Miglio, V. Brousseau-Couture, E. Godbout, G. Antonius, Y.-H. Chan, S. G. Louie, M. Côté, M. Giantomassi, and X. Gonze, “Predominance of non-adiabatic effects in zero-point renormalization of the electronic band gap,” *npj Comput. Mater.* **6** (2020), 10.1038/s41524-020-00434-z.
- ⁶⁵C. Sousa and F. Illas, “On the accurate prediction of the optical absorption energy of F-centers in MgO from explicitly correlated ab initio cluster model calculations,” *J. Chem. Phys.* **115**, 1435–1439 (2001).
- ⁶⁶E. Ertekin, L. K. Wagner, and J. C. Grossman, “Point-defect optical transitions and thermal ionization energies from quantum Monte Carlo methods: Application to the *f*-center defect in MgO,” *Phys. Rev. B* **87**, 155210 (2013).
- ⁶⁷Y. Chen, J. L. Kolopus, and W. A. Sibley, “Luminescence of the *f*⁺ center in MgO,” *Phys. Rev.* **186**, 865–870 (1969).
- ⁶⁸L. A. Kappers, R. L. Kroes, and E. B. Hensley, “*F*⁺ and *F*[′] centers in magnesium oxide,” *Phys. Rev. B* **1**, 4151–4157 (1970).
- ⁶⁹B. D. Evans and J. C. Kemp, “Vibronic aspects of the CaO and MgO *f* bands,” *Phys. Rev. B* **2**, 4179–4189 (1970).
- ⁷⁰V. Dobrovitski, G. Fuchs, A. Falk, C. Santori, and D. Awschalom, “Quantum control over single spins in diamond,” *Annu. Rev. Condens. Matter Phys.* **4**, 23–50 (2013).
- ⁷¹H. R. Phillip and E. A. Taft, “Kramers-Kronig analysis of reflectance data for diamond,” *Phys. Rev.* **136**, A1445–A1448 (1964).
- ⁷²R. Q. Hood, P. R. C. Kent, R. J. Needs, and P. R. Briddon, “Quantum Monte Carlo study of the optical and diffusive properties of the vacancy defect in diamond,” *Phys. Rev. Lett.* **91**, 076403 (2003).
- ⁷³C. D. Clark, J. Walker, and R. W. Ditchburn, “The neutral vacancy in diamond,” *Proc. R. Soc. A: Math. Phys. Sci.* **334**, 241–257 (1973).
- ⁷⁴G. Davies, “The jahn-teller effect and vibronic coupling at deep levels in diamond,” *Rep. Prog. Phys.* **44**, 787–830 (1981).
- ⁷⁵J. C. A. Prentice, B. Monserrat, and R. J. Needs, “First-principles study of the dynamic Jahn-Teller distortion of the neutral vacancy in diamond,” *Phys. Rev. B* **95**, 014108 (2017).
- ⁷⁶W. C. Mackrodt, F. S. Gentile, and R. Dovesi, “The calculated energies and charge and spin distributions of the excited GR1 state in diamond,” *J. Chem. Phys.* **156**, 044708 (2022).
- ⁷⁷C. D. Clark, R. W. Ditchburn, and H. B. Dyer, “The absorption spectra of natural and irradiated diamonds,” *Proc. R. Soc. A: Math. Phys. Sci.* **234**, 363–381 (1956).
- ⁷⁸M. Lannoo and A. Stoneham, “The optical absorption of the neutral vacancy in diamond,” *J. Phys. Chem. Solids* **29**, 1987–2000 (1968).